THE JOURNAL OF BIOLOGICAL CHEMISTRY
Vol. 279, No. 1, Issue of January 2, pp. 363–373, 2004

Printed in U.S.A.

Structures of γ-Aminobutyric Acid (GABA) Aminotransferase, a Pyridoxal 5′-Phosphate, and [2Fe-2S] Cluster-containing Enzyme, Complexed with γ-Ethynyl-GABA and with the Antiepilepsy Drug Vigabatrin*

Received for publication, June 4, 2003, and in revised form, October 3, 2003
Published, JBC Papers in Press, October 8, 2003, DOI 10.1074/jbc.M305884200

Paola Storici‡§, Daniela De Biase¶‖, Francesco Bossa¶‖, Stefano Bruno, Andrea Mozzarelli**, Caroline Peneff‡, Richard B. Silverman‡‡§§, and Tilman Schirmer‡¶¶**

*From the ‡Division of Structural Biology, Biozentrum, University of Basel, Switzerland, the ¶Department of Biochemical Sciences A. Rossi Fanelli and ‖Centro di Eccellenza di Biologia e Medicina Molecolare, University of Rome La Sapienza, 00185 Roma, Italy, the **Department of Biochemistry and Molecular Biology, and National Institute for the Physics of Matter, University of Parma, 43100 Parma, Italy, the ‡‡Department of Chemistry, Department of Biochemistry, Molecular Biology, and Cell Biology, and the Drug Discovery Program, Northwestern University, Evanston, Illinois 60208-3113*

γ-Aminobutyric acid aminotransferase (GABA-AT) is a pyridoxal 5′-phosphate-dependent enzyme responsible for the degradation of the inhibitory neurotransmitter GABA. GABA-AT is a validated target for antiepilepsy drugs because its selective inhibition raises GABA concentrations in brain. The antiepilepsy drug, γ-vinyl-GABA (vigabatrin) has been investigated in the past by various biochemical methods and resulted in several proposals for its mechanisms of inactivation. In this study we solved and compared the crystal structures of pig liver GABA-AT in its native form (to 2.3-Å resolution) and in complex with vigabatrin as well as with the close analogue γ-ethynyl-GABA (to 2.3 and 2.8 Å, respectively). Both inactivators form a covalent ternary adduct with the active site Lys-329 and the pyridoxal 5′-phosphate (PLP) cofactor. The crystal structures provide direct support for specific inactivation mechanisms proposed earlier on the basis of radiolabeling experiments. The reactivity of GABA-AT crystals with the two GABA analogues was also investigated by polarized absorption microspectrophotometry. The spectral data are discussed in relation to the proposed mechanism. Intriguingly, all three structures revealed a [2Fe-2S] cluster of yet unknown function at the center of the dimeric molecule in the vicinity of the PLP cofactors.

Two important neurotransmitters involved in the regulation of brain neuronal activity are γ-aminobutyric acid (GABA),[1] one of the most widely distributed inhibitory neurotransmitters, and L-glutamic acid, an excitatory neurotransmitter (1). The concentration of GABA is regulated by two pyridoxal 5′-phosphate (PLP)-dependent enzymes, L-glutamic acid decarboxylase, which catalyzes the conversion of L-glutamate to GABA, and GABA aminotransferase (GABA-AT, EC 2.6.1.19), which degrades GABA to succinic semialdehyde (2). GABA-AT is a homodimer with each subunit containing an active-site PLP covalently bound to Lys-329 via a Schiff base. The primary sequence of GABA-AT has been deduced from the cDNA of pig brain (3) and from peptide fragments of the pig liver enzyme (4). Together with the structurally well characterized enzymes ornithine aminotransferase (OAT) and dialkylglycine decarboxylase (DGD), GABA-AT belongs to the subfamily II of the α-family of PLP-dependent enzymes (5). In 1999, the x-ray crystal structure of pig liver GABA-AT was reported at 3.0-Å resolution (6), which elucidated the active-site geometry and allowed conclusions to be drawn with respect to its specificity. The mechanism for GABA-AT is well known (7). GABA is transaminated to succinic semialdehyde, thereby converting the pyridoxal 5′-phosphate (PLP) cofactor to its pyridoxamine 5′-phosphate (PMP) form. In the reverse half-reaction the enzyme is regenerated by conversion of α-ketoglutarate to glutamate.

When the concentration of GABA diminishes below a threshold level in the brain, convulsions result (8), raising the brain GABA levels terminates the seizure (9). The incidence of seizure activity is very prevalent in the world. In fact, when epilepsy is defined broadly as any disease characterized by recurring convulsive seizures, then almost 1% of the entire world population can be classified as having epilepsy (10). Consequently, anticonvulsant agents have been sought for centuries. Not until diphenylhydantoin (Dilantin) was introduced onto the drug market over 65 years ago was any particular anticonvulsant drug widely used (11). However, this drug is not generally applicable. In fact, about one-quarter of epileptic patients worldwide (about 12 million people) do not respond to any marketed anticonvulsant drug. Therefore, the need for new anticonvulsant drugs is great (10).

A reduction in the concentrations of GABA has been implicated not only in the symptoms associated with epilepsy (12,

* This work was supported by the National Institutes of Health Grant NS15703 (to R. B. S.), by Italian Ministero dell'Istruzione, dell'Università e della Ricerca (Grant COFIN2001-2002) (to A. M. and F. B.), and by Italian Consiglio Nazionale delle Ricerche, Progetto Finalizzato Biotecnologie (Grant 99.00306.49.PF49). The costs of publication of this article were defrayed in part by the payment of page charges. This article must therefore be hereby marked "*advertisement*" in accordance with 18 U.S.C. Section 1734 solely to indicate this fact.

The atomic coordinates and structure factors (code 1ohv, 1ohy, 1ohw) have been deposited in the Protein Data Bank, Research Collaboratory for Structural Bioinformatics, Rutgers University, New Brunswick, NJ (http://www.rcsb.org/).

§ Current address: Dept. of Biology, Discovery Research Oncology, Pharmacia Corp., Viale Pasteur 10, 20014 Nerviano, Italy.

§§ To whom correspondence may be addressed: Dept. of Chemistry, Northwestern University, Evanston, IL 60208-3113. Tel.: 847-491-5653; Fax: 847-491-7713; E-mail: Agman@chem.northwestern.edu.

¶¶ To whom correspondence may be addressed: Biozentrum, University of Basel, Klingelbergstrasse 50–70, CH-4056 Basel, Switzerland. Tel.: 41-61-267-2089; Fax: 41-61-267-2109; E-mail: tilman. schirmer@unibas.ch.

[1] The abbreviations used are: GABA, γ-aminobutyric acid; GABA-AT, γ-aminobutyric acid aminotransferase; OAT, ornithine aminotransferase; DGD, dialkylglycine decarboxylase; PLP, pyridoxal 5′-phosphate; PMP, pyridoxamine 5′-phosphate; AAT, aspartate aminotransferase; GEG, γ-ethynyl-GABA, 4-amino-5-hexynoic acid; r.m.s.d., root mean square deviation.

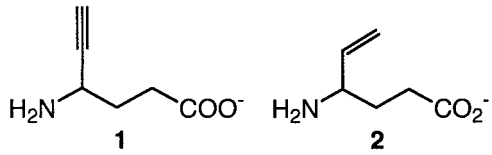

STRUCTURES 1 AND 2

13) but also with several other neurological diseases such as Huntington's chorea (14), Parkinson's disease (15), Alzheimer's disease (16), and tardive dyskinesia (17). Administration of GABA peripherally is not effective, because GABA, under normal conditions, cannot cross the blood-brain barrier; however, several other approaches have been taken to increase the brain concentrations of GABA. One approach is the use of a compound that crosses the blood-brain barrier and then selectively inhibits or inactivates GABA-AT, thereby causing a buildup of GABA. Numerous competitive inhibitors of GABA-AT, particularly compounds having a backbone structure similar to GABA (18–23), and a variety of mechanism-based inactivators (24) of GABA-AT (25) show anticonvulsant activity. The earliest analog reported was 4-amino-5-hexynoic acid (**1**, γ-ethynyl GABA, GEG), which did not become a clinical candidate (25). The corresponding alkene, 4-amino-5-hexenoic acid (**2**, γ-vinyl GABA, vigabatrin) (26), was the most effective of these mechanism-based inactivators as an anticonvulsant agent.

Vigabatrin (**2**), which has high potency (27), has been shown to be an effective treatment for epilepsies that are resistant to other anticonvulsant drugs (28) and currently is used in over 60 countries worldwide (but not in the U. S., where it is presently at the pre-registration status for treatment of infantile spasms). However, about 0.5 g of this drug has to be taken daily to be efficacious. As with all psychotropic drugs, there are a variety of side effects, most severe in this case is a visual field defect (29), which restricts the monotherapy of vigabatrin to refractory epilepsy. The drug is sold as a racemic mixture, and it is not known how many of the side effects arise from the administration of the inactive enantiomer (*R*-isomer). Other mechanism-based inactivators of GABA-AT, such as gabaculine (30, 31) and ethanolamine-*O*-sulfate (32), are generally toxic, nonspecific, and/or cross the blood-brain barrier poorly.

Recently, it was found that vigabatrin possesses another remarkable activity: it prevents addiction to various abusive substances in rats and baboons (33). The mechanism was determined to be the same as that for epilepsy, namely increasing the GABA concentration in the brain by inactivating GABA-AT. Increased GABA levels antagonize the extracellular dopamine levels responsible for drug addiction. New inhibitors that are in particular more potent and lipophilic, that is so they can more easily cross the blood-brain barrier, are needed.

Two mechanisms were proposed for inactivation of GABA-AT by GEG (34); these are shown in Schemes 1 and 2. For inactivation by vigabatrin, three different potential mechanisms (shown in Schemes 3 and 4) were suggested, based on spectroscopic and radiolabeling evidence (35), chemical intuition (26, 36), and extensive radiochemical experiments (37). The controversy regarding the inactivation mechanisms and structures of the covalent adducts could be settled with crystal structures of these inactivators bound to GABA-AT.

Here, we have been able to use crystallography and polarized absorption microspectrophotometry to differentiate the inactivation mechanisms and adduct structures for the two mechanism-based inactivators of GABA-AT, GEG (**1**), and vigabatrin (**2**). Moreover, we report the presence of a [2Fe-2S] cluster at the center of the dimer, observed in the complex structures as well as in the native enzyme at 2.3-Å resolution.

MATERIALS AND METHODS

Crystallography—Pig liver GABA-AT was purified as described previously (35). Crystals of native enzyme were grown at room temperature in sitting drops by vapor diffusion and microseeding. The protein solution (10–14 mg/ml in 40 mM sodium acetate, pH 5.4) was mixed in a 1:1 ratio with precipitant solution containing 16–18% polyethylene glycol4000, 0–10% glycerol, and 50 mM sodium cacodylate, pH 6.0, and 1 mM dithiothreitol.

The GEG-inactivated GABA-AT crystals were obtained by overnight soaking of native crystals in a solution containing 10 mM GEG. Vigabatrin-inactivated GABA-AT crystals were obtained by pre-treatment of native GABA-AT with 10 mM vigabatrin for 1 h prior to crystallization. Each data set was obtained from a single flash-cooled crystal using either 10% ethylene glycol or Panjelly™ (Jena Bioscience) as cryoprotectants. Only a few cycles of crystal annealing were performed to improve crystal mosaicity. Data were collected on MAR image plates, processed with MOSFLM, and scaled with SCALA from the CCP4 suite (38). The models were refined with REFMAC5, including TLS refinement (39). Strong non-crystallographic symmetry restraints were imposed on the positional and thermal parameters of the four monomers in the asymmetric unit. In the initial rounds of refinement, the cofactor and Lys-329 were set as dummy values. This was followed by cyclic averaging using DM (40) to obtain the best unbiased map for interpretation of the adducts. After model building, refinement of the final model was performed without torsional angle restraints on the linkages between Lys-329, cofactor, and the inhibitor moiety. Planarity was imposed on the atoms of the pyridine ring, the carboxylate group, and, in case of the GEG complex, on the atoms belonging to the planar system of the CA=C double bond.

Chemical Analysis of Iron and Sulfur Content—The amount of iron bound to GABA-AT was determined colorimetrically, by using the iron chelator ferrozine (41). GABA-AT (5–10 μM, 460 μl) was mixed with ultrapure concentrated HCl (100 μl) and was incubated at 80 °C for 20 min with periodic vortexing. Following centrifugation at 15,000 rpm for 5 min to pellet the denatured protein, the supernatant (510 μl) was mixed with 10 mM ferrozine (20 μl) and 75 mM ascorbic acid (20 μl). To allow ferrozine chelation, the mixture was neutralized with saturated ammonium acetate and incubated for 20 min at room temperature. The absorbance at 562 nm of the newly formed magenta $Fe(ligand)_3^{2+}$ species was determined, and the iron concentration was calculated using the extinction coefficient for ferrozine, $\epsilon = 27{,}900\ M^{-1}\ cm^{-1}$ (41). Acid-labile inorganic sulfide was determined by the method of King and Morris (42).

Crystal Microspectrometry—Crystals of GABA-AT were stored at 15 °C in a stabilizing solution containing 22% (w/v) polyethylene glycol 4000, 50 mM sodium citrate, and 1 mM dithiothreitol at pH 5.6. The GABA-AT complexes were produced by soaking single crystals in the stabilizing solution containing 100 mM GEG or 10 mM vigabatrin, respectively. Crystals were loaded in a quartz flow cell that was mounted on the thermostated stage of a Zeiss MPM03 microspectrophotometer, equipped with a ×10 UV-visible Ultrafluar objective. Single crystal absorption spectra were collected in the range 300–700 nm with the electric vector of the linearly polarized light parallel and perpendicular to the extinction directions, as previously described (43, 44). The isotropic crystal spectrum A_i of GABA-AT was calculated according to $A_i = 1/3(A_x + A_y + A_z)$, where A_x, A_y, and A_z are the spectra recorded along the three perpendicular extinction directions (45).

Coordinates—The coordinates for native GABA-AT, and its complex structures with GEG and vigabatrin, have been deposited in the Rutgers Protein Data Bank (accession codes 1ohv, 1ohy, and 1ohw, respectively).

RESULTS

Overall Structure—The quality of the native GABA-AT data (2.3 Å) has been considerably improved since the previous study (6) due to better crystal order, use of flash-cooled crystals, and data acquisition at a synchrotron radiation source. Crystallographic details are given in Table I. The new structure confirms the previous model. The asymmetric unit contains two physiological dimers (AB and CD) with C2 symmetry. The two dimers superimpose with an r.m.s.d. of 0.23 Å, and the four subunits show pairwise r.m.s.d. values between 0.18 and 0.30 Å. This indicates that, within the limits of error, there is no structural asymmetry between the four different copies in the crystallographic asymmetric unit. Also, considering the

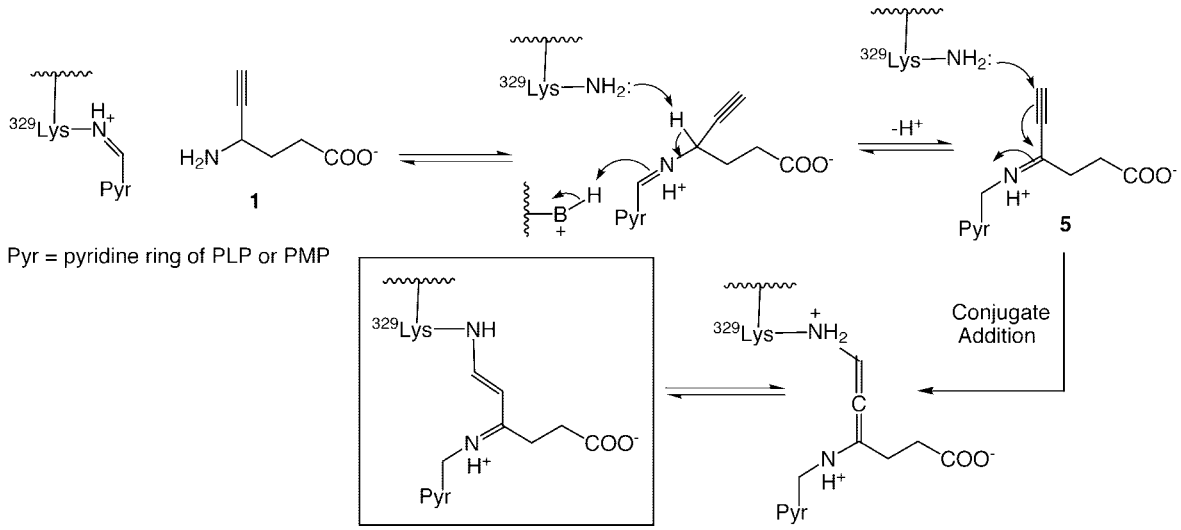

SCHEME 1

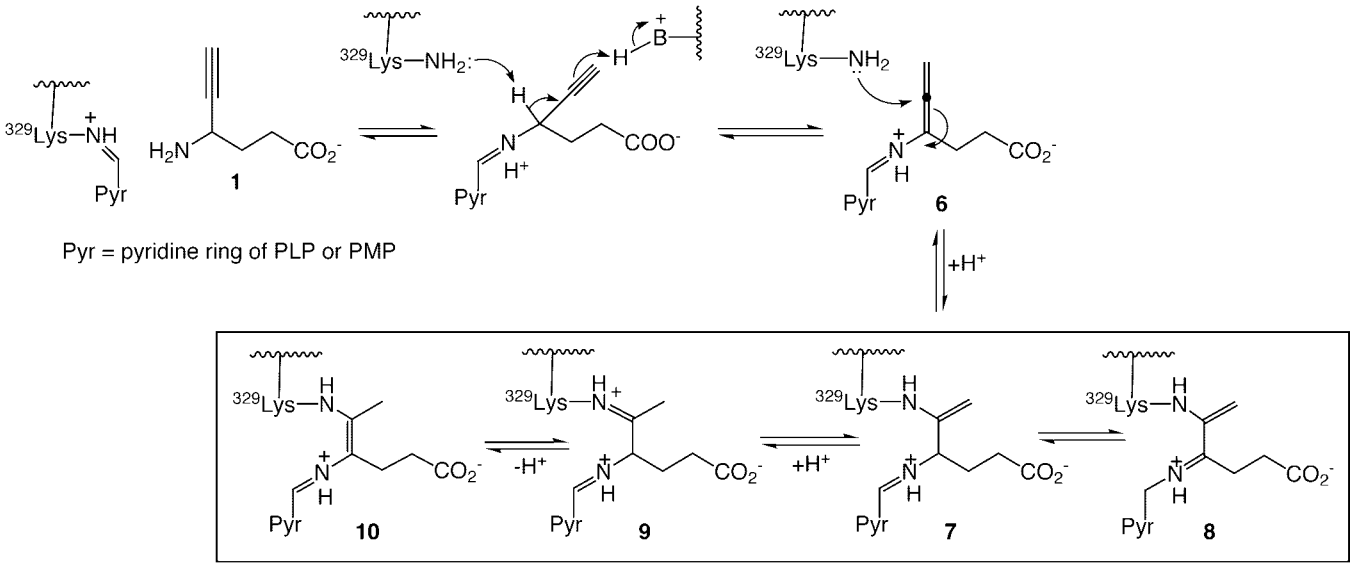

SCHEME 2

good quality of the overall crystallographic parameters (Table I), it appears unlikely that asymmetric dimers have been incorporated stochastically into the crystal lattice. Refinement of global temperature factors (TLS refinement), however, revealed that AB is the more mobile dimer within the crystal lattice. After TLS refinement, the remaining (intrinsic) *B*-factors of the subunits were virtually identical. This allowed the imposition of strong NCS constraints not only on the positional parameters but also on the individual *B*-factors.

The Native Cofactor: Structure and Absorption Spectrum—All four copies of the PLP cofactor in the asymmetric unit form a Schiff base linkage with Lys-329 (Fig. 1) and exhibit similar *B*-factors (between 15 and 20 Å^2) after TLS refinement. With a torsional angle κ (for torsion angle definition and atom nomenclature see Fig. 4*C*) of 23° ± 3° the Schiff's base nitrogen is roughly in the plane of the pyridine ring and forms a short H-bond with the pyridine oxygen (O3) indicative of a protonated aldimine. The torsional angle around the formal C4′=N double bond is 140° ± 2°. Thus, the conformation appears to be rather strained.

Single crystal polarized absorption spectra of GABA-AT, recorded along three perpendicular directions (Fig. 2), exhibit an intense band centered at 412 nm. This band is usually attributed to the ketoenamine tautomer of the protonated internal aldimine (*i.e.* with the proton on the aldimine nitrogen). However, there is a second band centered between 333 and 338 nm. A band at a similar position has been found in several PLP-dependent enzymes (43, 46) and has been attributed to the enolimine tautomer of the internal aldimine (with the proton on the pyridine oxygen), a species stabilized by a more hydrophobic environment (47). Noteworthy, the position of the minor band changes with the polarization direction, which suggests that this band does not originate from a single electronic transition, but results from overlapping bands. The reconstructed isotropic spectrum of the crystal (Fig. 2, *inset*) is similar to the spectrum of the enzyme in solution (35) with respect to both the peak positions and relative intensities, indicating that crystallization did not perturb the coenzyme environment or the tautomeric equilibrium.

[2Fe-2S] Cluster—Unexpectedly, a [2Fe-2S] cluster was identified on the molecular 2-fold symmetry axis at the center of the dimer in all structures investigated (Fig. 3, *A* and *B*). Previously, it was not possible to resolve this feature because of poor resolution (3 Å) (6). Fig. 3*B* shows that cysteines 135 and 138 at the N-terminal end of helix 5 together with their symmetry related mates chelate the cluster. Each of the iron atoms

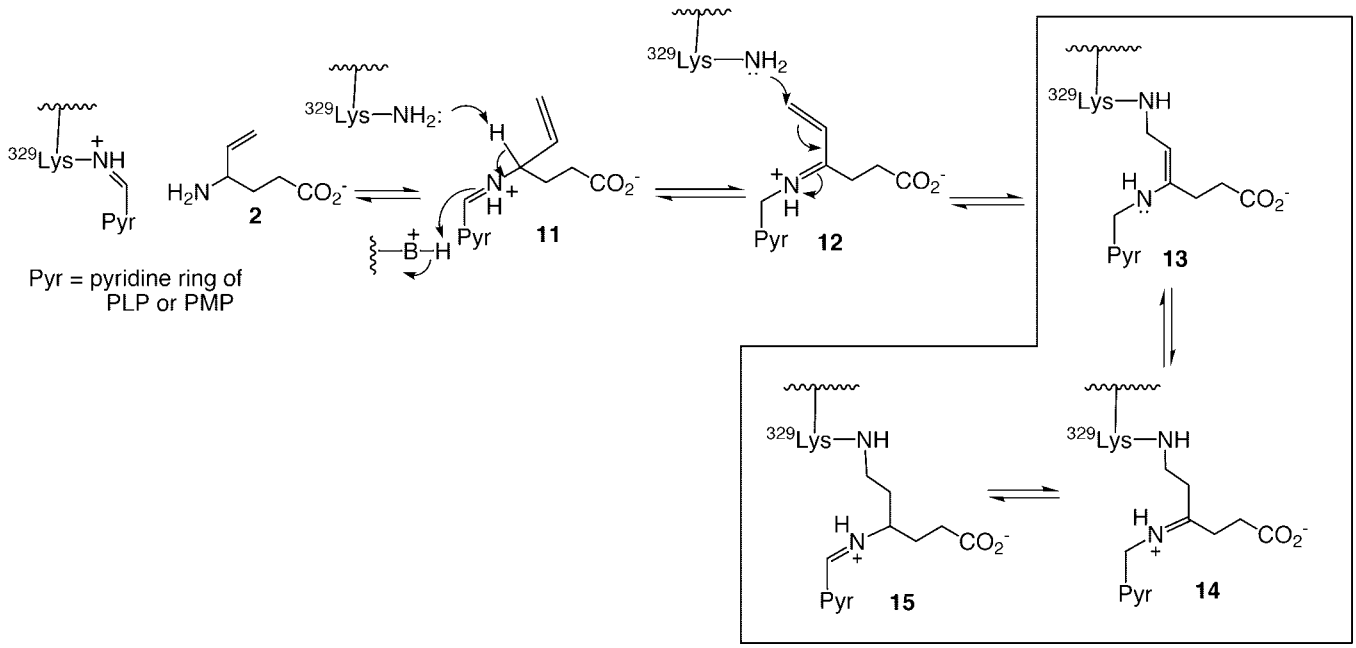

SCHEME 3

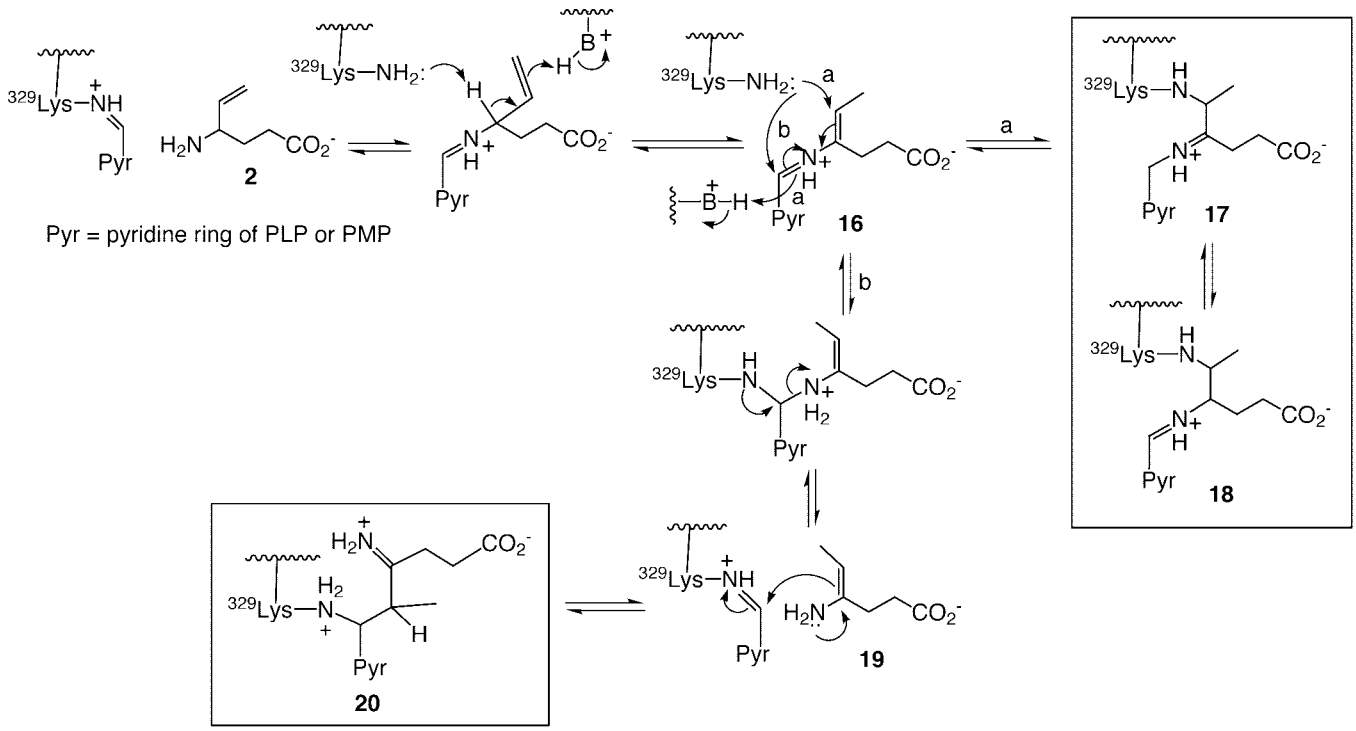

SCHEME 4

is coordinated tetrahedrally by two cysteines of one subunit and the two free sulfur atoms, which lie on the molecular 2-fold axis and cross-link to the symmetry related second iron atom. The Fe–S distances are 2.2–2.3 Å. The *B*-factors of the cluster atoms and the cysteines match well (differences < 4 Å^2).

A 2.3-Å anomalous difference density map computed with data collected at a wavelength of 0.98 Å (vigabatrin complex, cluster atoms omitted for phasing) shows peaks with a height $>$ 5 σ (Fig. 3*C*). The peaks are even more pronounced (>8 σ) in a map computed with data collected to the same resolution with CuK_α radiation at a home source (data not shown). This is to be expected for iron with its absorption edge at 1.7 Å and rules out the presence of zinc or other lighter elements.

Chemical analysis of the iron and acid-labile sulfide content of freshly purified GABA-AT corroborated the crystallographic interpretation. In four independent experiments, a content of 0.9–1.2 iron atoms per enzyme subunit was determined. The sulfide content was 0.8 and 0.9 (two experiments). In proteins, [2Fe-2S] clusters typically show absorption in the visible range of the spectrum with peaks around 330 nm, 420–460 nm, and a broad shoulder centered at 550 nm (48). Thus, in GABA-AT, any iron-sulfur cluster absorption will be largely concealed by the cofactor. A shoulder around 550–600 nm, however, is clearly visible in the crystal absorption spectrum (Fig. 2) as in solution (49). This is absent in the homologous OAT (49) that contains no FeS cluster.

TABLE I
Data collection and refinement statistics

The GABA-AT crystals are of space-group $P2_1$ and contain two dimers in the asymmetric unit.

Data set	Native	Vigabatrin complex	GEG complex
Sample	Native GABA-AT	GABA-AT co-crystallized with 10 mM vigabatrin	GABA-AT soaked in 10 mM GEG for 24 h
X-ray source; λ(Å)	ESRF, Grenoble; 0.984	Elettra, Trieste; 0.984	Rotating anode; 1.542
Unit cell: a, b, c (Å)	68.6, 225.0, 70.3	69.7, 226.7, 71.4	69.0, 225.9, 70.3
β (°)	108.4	108.8	108.5
Resolution range (Å)	30.0–2.3	30.0–2.3	30.0–2.8
Number of reflections	80,297	88,767	42,802
R_{sym} (%)[a]	8.5	7.3	9.8
$\langle I \rangle / \sigma(I)$	5.9	6.7	6.6
Completeness (%)	90.0	96.1	85.7
Multiplicity	2.0	2.2	2.5
R_{factor} (%)[b]	18.8	19.4	19.8
R_{free} (%)[c]	22.1	22.4	22.9
Number of protein atoms	29,216	29,216	29,216
Number of cofactor atoms	15	24	24
Number of FeS atoms	8	8	8
Number of water molecules	641	739	337
Mean overall *B*-factor (Å^2)[d]	24.0 (18.1)	26.3 (11.9)	25.9 (9.2)
r.m.s.d. bond lengths (Å)[e]	0.009	0.010	0.012
r.m.s.d. bond angles (°)[e]	1.1	1.2	1.4

[a] $R_{sym} = \Sigma_{hkl}\Sigma_i(|I(hkl) - \langle I(hkl)\rangle|)/\Sigma_{hkl}\Sigma_i \langle I(hkl)\rangle$.
[b] R_{factor} is the conventional *R* factor.
[c] R_{free} is the *R* factor calculated with 5% of the data that were not used for refinement.
[d] In *parentheses*, residual overall *B*-factor after TLS refinement.
[e] r.m.s.d. from ideal stereochemistry.

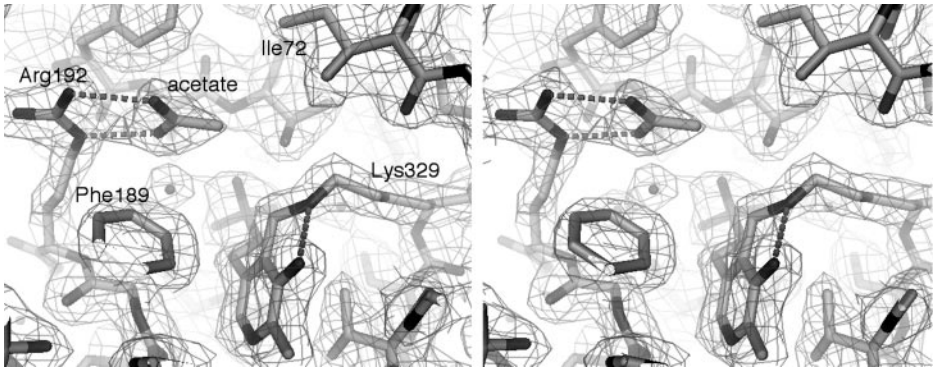

FIG. 1. **Stereographic projection of the active site of GABA-AT.** The final model is shown together with the $2F_o - F_c$ map (contour level, 1.2 σ). An acetate molecule is found close to Arg-192, *i.e.* at a position where the carboxylate moiety of the natural substrate GABA is expected to bind (6).

GABA-AT in Complex with GEG—The electron density map of GABA-AT obtained upon soaking of crystals with GEG, clearly shows a covalent modification at the active site (Fig. 4*A*). The internal aldimine linkage between Lys-329 and PLP of the native enzyme (Fig. 1) has been broken. Instead, a covalent ternary adduct is formed among the cofactor, the inhibitor, and the lysine residue. Fig. 4*C* demonstrates that the pyridine ring is only slightly tilted (about 5°) with respect to its native orientation. In accord with this, Phe-189 has moved by 0.6 Å. As anticipated earlier (6), the carboxylate group of the inhibitor forms a salt bridge with the guanidinium group of Arg-192, which is found pushed outwards by 0.7 Å when compared with the native enzyme.

The density shows that the distance between the two nitrogens (NZ and N) of the PLP-lysine linkage is spanned by three and not four bonds, thus indicating that the reaction has proceeded according to the mechanism depicted in Scheme 2 and not by the mechanism in Scheme 1. In fact, the map was best modeled with tautomer **10** of Scheme 2 (Fig. 4*A*), yielding a flat residual difference map. Missing density for the branching C′ atom in the unbiased map is probably the result of its modest resolution (2.8 Å) or some heterogeneity, *i.e.* the presence of some of the other tautomers shown in Scheme 2 (see "Discussion"). The distance of the branching methyl group to the Ile-72 side chain is rather short ranging from 3.0 to 3.3 Å in the individual active sites. The plane of the pyridine ring is roughly perpendicular to the plane defined by the CA=C double bond. The (unconstrained) C4–C4′–N–CA torsional angle around the formal C4′=N double bond is 155°. Both nitrogen atoms of the linkage (N and NZ) are in H-bonding distance to the pyridine O3.

The reaction of GEG with GABA-AT crystals was monitored by measuring polarized absorption spectra as a function of crystal-soaking time (Fig. 5*A*). A slow decrease of the band at 412 nm was observed with a concomitant increase of the band at 337 nm with an isosbestic point at about 370 nm, indicating the formation of an inhibitor·enzyme complex. The complex was found to be very stable (Fig. 5*A*, *inset*), as observed in solution,[2] suggesting an irreversible covalent linkage between GEG and the enzyme.

GABA-AT in Complex with Vigabatrin—Soaking of GABA-AT crystals in vigabatrin solution did not yield interpretable electron density for the adduct (see also below). Co-crystallization, however, yielded the structure depicted in Fig. 4*B*. Again, a ternary adduct among Lys-329, the cofactor, and the inhibitor has formed, but this time the electron density indicates the presence of four bonds joining N with NZ. Therefore, it can be ruled out that intermediates of the alternative Michael addition pathway and the enamine pathway (Scheme 4) are present in significant amounts. Instead, a model of the

[2] D. De Biase, unpublished results.

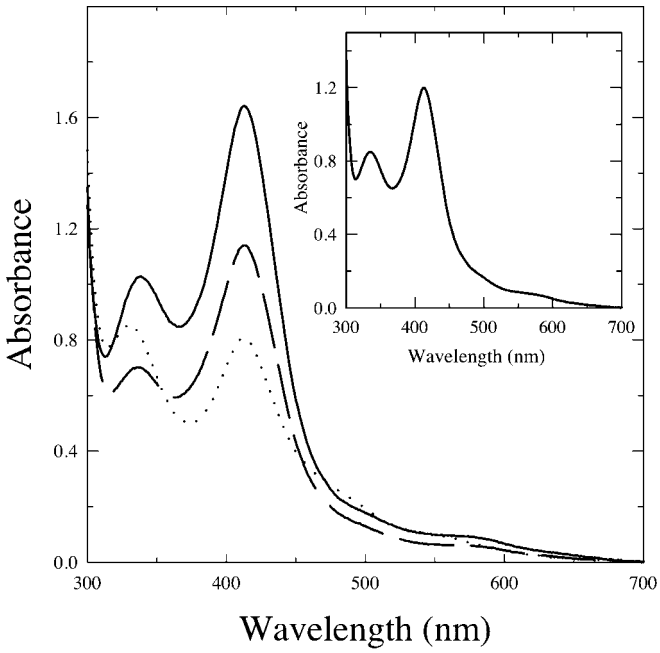

FIG. 2. **Polarized absorption spectra of native GABA-AT crystals.** Spectra were recorded with the polarization direction along the three mutually perpendicular extinction directions of the monoclinic GABA-AT crystals and are shown with distinct line-types. *Inset*, calculated isotropic spectrum.

external aldimine **15** that can occur after Michael addition at the terminal carbon of the vinyl group by the active site lysine (Scheme 3) fits the electron density best and yields a flat difference map. The adduct model is well accommodated in the active site of the enzyme with the NZ amino group forming an H-bond with the main-chain carbonyl of residue 72 and the aldimine NH, which lies in the plane of the pyridine ring forming an H-bond with O3. The adduct appears to be in a rather relaxed conformation with an (unconstrained) torsion angle around the C4′–N aldimine linkage of −169°.

To monitor the kinetics of the reaction in the crystal, polarized absorption spectra were acquired of GABA-AT crystals that were soaked in a vigabatrin solution (Fig. 5*B*). A gradual decrease in the band at 412 nm with a concomitant increase of the band at 337 nm was observed with an isosbestic point at 365 nm. The spectral changes were complete in about 3 h (Fig. 5*B*, *inset*). At longer times, a decrease of both band intensities was apparent, whereas their intensity ratio remained constant, probably indicating release of a modified cofactor from the crystal. The reaction appears to be irreversible, because the removal of the reagent after 9 h of incubation did not lead to a reversal of the spectral changes. When the reaction of the enzyme with vigabatrin is carried out in the presence of 10 mM α-ketoglutarate (to convert any PMP form back to the competent PLP form), the same spectral changes were observed, although at a slower rate (data not shown).

An attempt was made to follow these changes structurally by incubating GABA-AT crystals for a defined length of time before flash cooling and data acquisition. Several data sets were collected after incubation with vigabatrin for 3–24 h (data not shown). In all cases it was evident that a reaction had occurred as judged by the absence of a covalent aldimine linkage between C4′ of the cofactor and NZ of Lys-329 due to a motion of the tip of the lysine side-chain and a slight though significant tilt of the cofactor ring. Coarse modeling gave a C4′ to NZ distance of 2.5–3 Å, somewhat smaller than the corresponding distance (4.0 Å) in the vigabatrin co-crystallization complex (Fig. 4*B*). The remainder of the density did not allow unambiguous interpretation. In all cases, density was found close to Arg-192, probably representing the carboxylate group of the inhibitor. Addition of α-ketoglutarate did not alter the results significantly.

DISCUSSION

The [2Fe-2S] Cluster—An unexpected finding of the current study is the presence of an iron-sulfur cluster at the center of the GABA-AT dimer that is clearly resolved (Fig. 3). The presence of metals in mammalian GABA-AT, although suspected, was never reported in previous biochemical studies. The complexity of the visible absorption spectrum of GABA-AT was initially assigned to anomalous binding of PLP (50). Iron-sulfur clusters are well known in enzymology for their important functions in electron transfer processes, but they also are now known to catalyze dehydration reactions, to stabilize protein structure, to regulate metabolic pathways, to act as biological sensors of iron, molecular oxygen, and superoxide, nitric oxide and are involved in the formation of protein-bound radicals (51). In GABA-AT the [2Fe-2S] cluster cross-links the subunits of the physiological dimer. It appears unlikely that this is its only role, because structurally homologous proteins such as human OAT (52) and bacterial DGD (53) exhibit the same subunit organization, but lack a cross-linker at the dimer interface. The same is true for all other aminotransferases of known structure. To the best of our knowledge, there are no other iron-sulfur cluster-containing enzymes that have a cluster exclusively for subunit cross-linking. Iron-sulfur clusters can be destroyed by oxidation (for a review see Ref. 54) and can exert in this way a redox state sensing function. Because the iron-sulfur cluster of GABA-AT is observed without resorting to anaerobic conditions, its stability does not seem to be exquisitely sensitive to oxidation.

Interestingly, cysteines 135 and 138, which chelate the cluster, are conserved in the GABA-AT sequences of higher organisms, including *Drosophila*, but are not present in bacteria and yeast, with the exception of the basidiomycete *Ustilago maydis*. It is conceivable that during biogenesis the iron-sulfur cluster is needed for the proper association of GABA-AT subunits to form the functional dimer. This then may happen only in the strongly reducing environment of the mitochondria and would ensure that the enzyme becomes active only at its destination.

Alternatively, the redox state of the cluster may regulate indirectly the activity of the enzyme as suggested by the relatively short distance between the cluster and the two active sites (Fig. 3*B*). Most interestingly, a direct influence of nitric oxide (which is known to modulate the redox state of iron-sulfur clusters) on GABA-AT activity in rat brains has recently been reported (55). The presence of an iron-sulfur cluster in PLP enzymes has been recently observed in biotin synthase (56) and lysine 2,3-aminomutase (57). In these cases, the iron-sulfur cluster is directly involved in catalysis, which is not the case for GABA-AT. Clearly, *in vitro* studies have to be performed to characterize and to clarify the role of the [2Fe-2S] cluster in mammalian GABA-AT.

Native Structure and Cofactor Spectrum—In the native enzyme, the PLP cofactor is bound to Lys-329 via a Schiff base linkage, and there is no evidence for a structural asymmetry between the active sites of the dimer as previously reported (50). The short distance between the aldimine N and the pyridine O3′ indicates that the cofactor is protonated. The aldimine linkage appears strained, because the conjugated systems of the cofactor ring and the linkage are not coplanar (with the aldimine N having a distance of 0.6 Å to the cofactor plane, Fig. 1). This strained conformation is observed in several PLP enzymes, *e.g.* in tryptophan synthase (58) (PDB code 1QOP, struc-

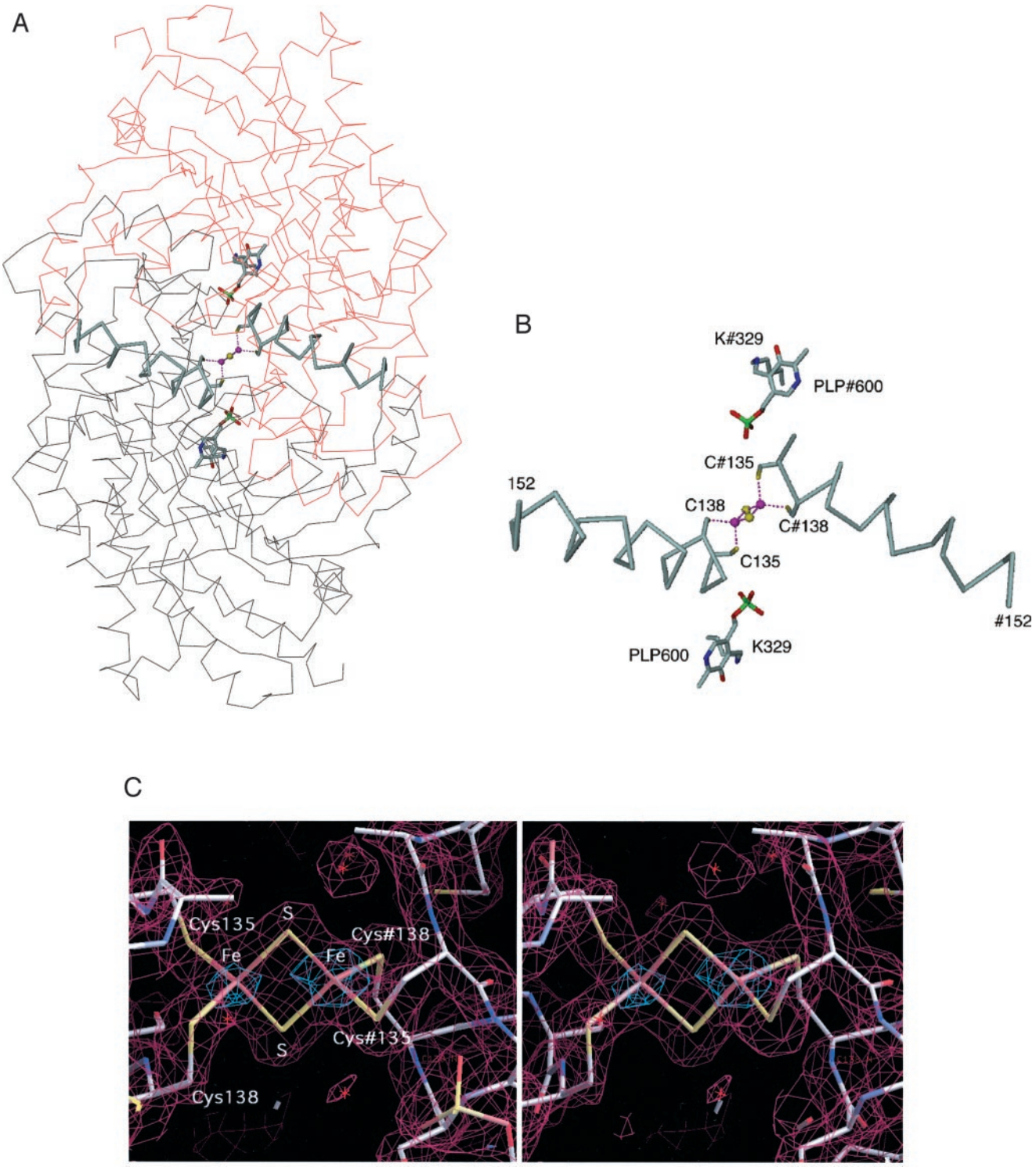

FIG. 3. **The [2Fe-2S] cluster at the center of the GABA-AT dimer.** *A*, structure of the GABA-AT dimer. The view is approximately along the molecular 2-fold symmetry axis. The Cα traces of the two subunits are shown in *black* and *red*. Helix 5 and its symmetry mate are highlighted by *thick gray traces*. The [2Fe-2S] cluster on the molecular 2-fold symmetry axis together with the liganding cysteines and the two symmetry related PLP cofactors are shown in full view. *B*, close-up view of *A*. The Cα traces have been omitted for clarity. Symmetry-related residues are marked with the symbol "#." *C*, stereographic close-up view. The molecular 2-fold axis is approximately along the vertical direction. The native $2F_o - F_c$ omit map (*magenta*; contour level 1.2 σ) and the anomalous difference map (*light blue*; contour level 4.5 σ) were computed with data to 2.3-Å resolution (data set of the vigabatrin complex). The iron and sulfur atoms were not included for phasing.

ture determined to 1.4-Å resolution) and should be important to catalysis by raising the ground state energy of the aldimine (59).

It is known that the GABA-AT cofactor does not titrate between pH 5.5 and 9 (60), *i.e.* the aldimine N has a pK_a above 9. In aspartate aminotransferase (AAT), which titrates in the neutral pH range, the deprotonated aldimine double bond is rotated out of the ring plane (κ about 80° (61)). A similar rotation is prevented by the presence of Val-300 (which corresponds to Ala-224 in AAT), and this may explain the high pK_a value of the cofactor. The absence of an equivalent of AAT Tyr-225, which can stabilize the uncompensated single charge

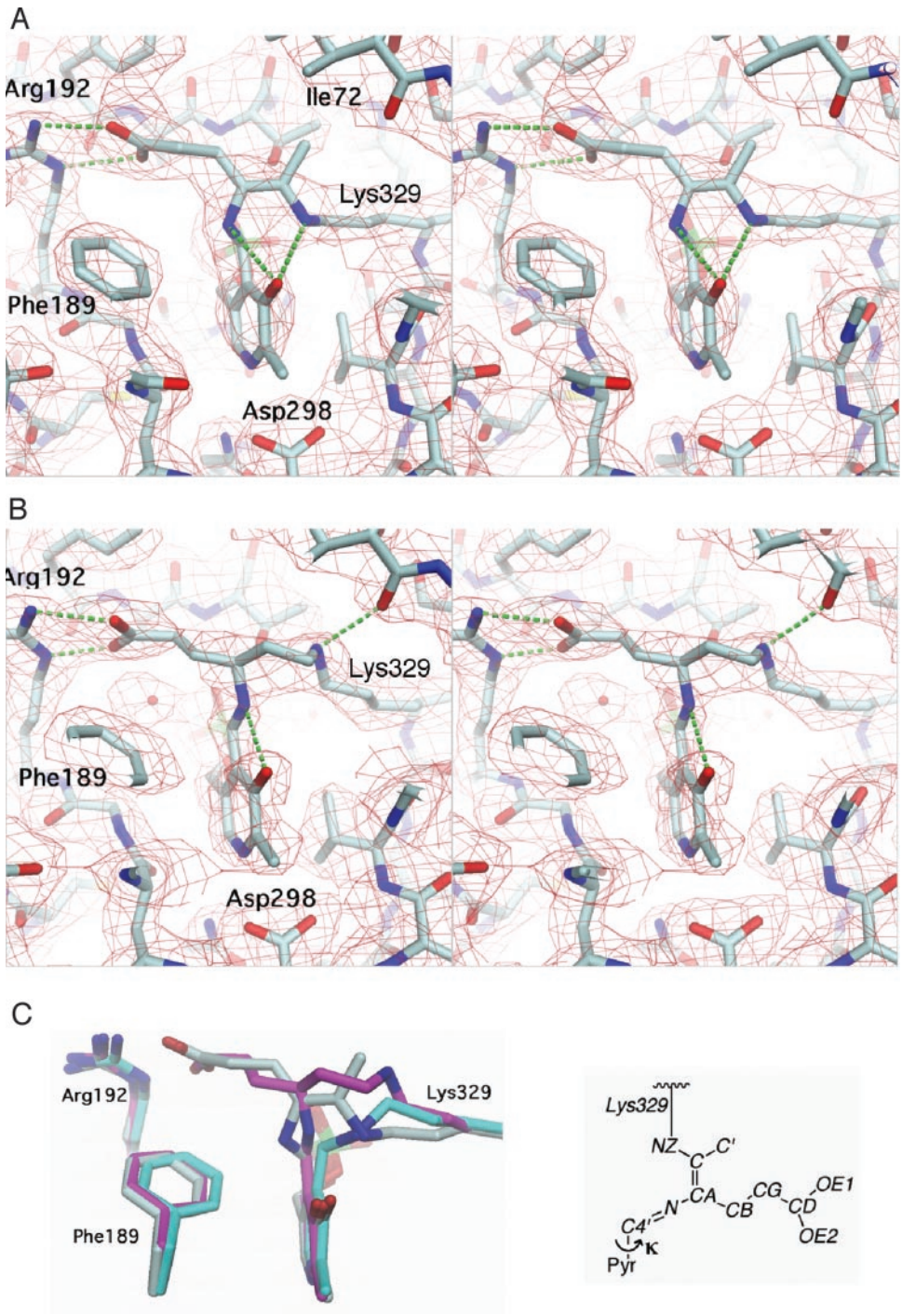

FIG. 4. *A*, stereographic projection of the active site of GABA-AT after chemical modification with GEG. The final model is shown together with the cyclic averaged omit maps (contour level, 1.0 σ). The ternary adduct has been modeled according to structure **10** of Scheme 2. *B*, stereographic projection of the active site of GABA-AT after chemical modification with vigabatrin. The final model is shown together with the cyclic averaged omit maps (contour level, 1.0 σ). The ternary adduct has been modeled according to structure **15** of Scheme 3. *C*, comparison of adduct structures. The models of the native PLP cofactor forming an aldimine linkage with Lys-329 (carbon atoms colored in *cyan*) of the ternary adduct in the GABA-AT·GEG complex (carbons in *gray*), and of the ternary adduct in the GABA-AT·vigabatrin complex (carbons in *magenta*) are shown. For this comparison the active-site protein residues have been *superimposed*. Side chains Phe-189 and Arg-192 are found slightly shifted upon formation of the ternary complexes. The schematic drawing defines the torsional angle κ and the nomenclature of the atoms.

on the pyridine O3 in AAT, offers another possible explanation.

The visible absorption spectrum (Fig. 2) shows two peaks as have also been observed for the PLP forms of AAT at low pH (62) and of tryptophan synthase (43). These can tentatively be assigned to the protonated aldimine in the ketoenamine (λ_{max} = 412 nm) and enolimine (λ_{max} ~ 335 nm) form. Another interpretation would be that the non-coplanarity of the PLP ring and the aldimine linkage can cause the occurrence of two electronic transitions for the ketoenamine form, as has been demonstrated by Clark *et al.* (62). Their semiempirical calculations showed that the positions of the absorption bands vary with the torsional angle κ and can fall in a range that is observed for GABA-AT (and other PLP enzymes). In the crystal spectrum (Fig. 2), the polarization ratios differ for the two bands, which is consistent with a different orientation of the coenzyme in the ketoenamine and enolimine tautomers and/or

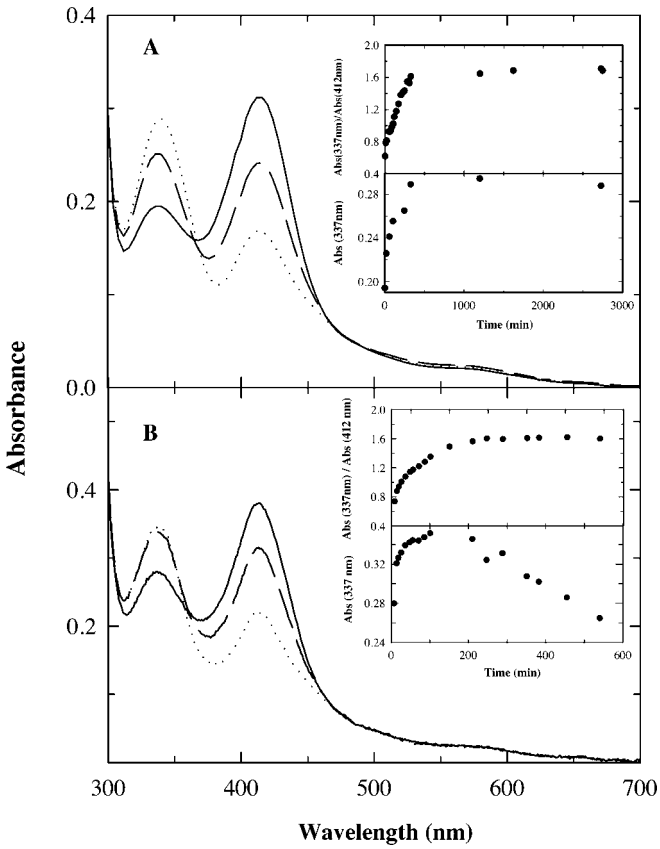

FIG. 5. **Polarized absorption spectra of GABA-AT crystals in the presence of GEG and vigabatrin.** Spectra were recorded with light linearly polarized along the crystal extinction direction with higher absorption intensity. *A*, spectra measured in the absence (*solid lines*) and presence of 100 mM GEG after 90 min (*dashed lines*) and 1200 min (*dotted lines*). *B*, spectra measured in the absence (*solid lines*) and presence of 10 mM vigabatrin after 30 min (*dashed lines*) and 180 min (*dotted lines*). The *insets* show the time course of the $A_{337\ nm}/A_{412\ nm}$ peak absorption ratio and the $A_{337\ nm}$ peak absorption.

different directions of the dipole transition moments. The variability of the position of the peak assigned to the enolimine tautomer with polarization direction suggests that this band does not originate from a single electronic transition. Whether this results from a contribution of the iron-sulfur cluster has yet to be investigated.

Inactivation by GEG—This study is part of a project to unravel the structure and function of GABA-AT for the development of inhibitory drugs to control GABA levels in the brain. A first result in this direction has been published recently (63). GEG (**1**), one of the first rationally designed mechanism-based inactivators, was shown to be a potent inactivator of GABA-AT (30, 64, 65). *In vivo*, GEG causes a long-lasting decrease in mouse brain GABA-AT activity in a dose-dependent manner when administered peripherally and has been shown to increase synaptosomal GABA levels (66, 67).

Two inactivation mechanisms for GEG have been reported (34). In Scheme 1, following Schiff base formation with the active site PLP, γ-(CA)-proton removal and tautomerization into the cofactor gives the α,β-ethynyliminium complex (**5**), a highly electrophilic species, which would undergo reaction at the terminal carbon atom of the ethynyl group (36) with Lys-329. Scheme 2 is similar to Scheme 1 except after γ-(CA)-proton removal, tautomerization occurs with the ethynyl group to give **6**, a conjugated allene, which can undergo reaction at the penultimate carbon with the active site lysine residue (34, 36, 64) (at the time of publication it was not known that the nucleophile is Lys-329, as shown in Schemes 1 and 2).

These two mechanisms, which differ in the point of attachment of Lys-329 to the inactivator, have now been differentiated by crystallography (Fig. 4*A*). Lys-329 was found to be attached to the penultimate carbon, thereby supporting the overall mechanism in Scheme 2. Attack of **6** by Lys-329 can lead to four different tautomers (**7**-**10**). Following inactivation of [7-^{3}H]PLP-reconstituted GABA-AT by GEG and denaturation, PLP was released, which is consistent only with **7**, **9**, and **10** (34).

On steric grounds, as well as the [7-^{3}H]PLP experiment described above, structure **8** is highly unlikely, because it is not possible to bring the C4′ of the coenzyme into the plane defined by the ketimine double bond. Modeling of the remaining tautomers (**7**, **9**, and **10**) and subsequent refinement yielded comparable fits with the density. The well defined positions of the PLP cofactor, the lysine side chain, and the inhibitor cofactor (Fig. 4*A*) impose strong constraints on the geometry of the linkage. For adducts **7** and **9**, the distance between NZ and C4′ is 2.1–2.4 Å (depending on the subunit), which is unreasonably close. This distance is increased to 2.5–2.6 Å for adduct **10**. Although still rather strained, this tautomer clearly represents the best fit of the structural data. Credence to this interpretation is given also by the close to planar torsional angle around the aldimine double bond. The crystal structure, therefore, clearly confirms the mechanism proposed based on radiolabeling experiments (34). The crystal absorption spectrum of GABA-AT after incubation with GEG (Fig. 5*A*) shows the two bands of the native spectrum (Fig. 2), although with a change in relative height. Thus, the spectrum is compatible with the aldimine **10**, with a shifted ketoenamine/enolimine equilibrium compared with the native structure. The CA=CB double bond probably does not contribute to the visible spectrum, because its orientation is roughly perpendicular to the pyridine plane. The presence of other ternary adducts of Scheme 2, however, cannot be ruled out. The reaction proceeds more slowly than that with vigabatrin (see below), leading to the formation of a stable complex, as observed in solution. This is consistent with the observed covalent link between the inhibitor, the PLP, and the protein.

Inactivation by Vigabatrin—Three different inactivation mechanisms for GABA-AT by vigabatrin (**2**) have been reported (Schemes 3 and 4). One mechanism (Scheme 3) involves azallylic isomerization followed by γ-proton removal as in the normal catalytic mechanism with substrate. Unlike GABA, vigabatrin is converted into an electrophilic species (**12**), which could undergo Michael addition at the terminal carbon of the vinyl group by the active site Lys-329 to give **13**. Adduct **13** can easily be tautomerized to **14** or **15**. An alternative Michael addition pathway (Scheme 4) requires allylic isomerization through the vinyl double bond to give **16**, which also is a Michael acceptor. This can be attacked by Lys-329 to give attachment of the nucleophile at the penultimate carbon of the former vinyl group to yield **17** and **18** (path a). Or, alternatively, Lys-329 can attack the PLP imine carbon rather than undergoing Michael addition, leading to enamine **19**, which can condense with the PLP imine to give adduct **20** (path b).

Lippert *et al.* (26) proposed the mechanism in Scheme 3 up to intermediate **13**. Metcalf (36) suggested two possibilities: Scheme 3 up to intermediate **13** and the mechanism in Scheme 4 to give **17**. On the basis of [^{14}C]vigabatrin labeling experiments and mass spectrometry on the radiolabeled peptide, De Biase *et al.* (35) ruled out the enamine mechanism (Scheme 4, *path b*), because no coenzyme was detected in the peptide-inhibitor adduct. They suggested that their data were consistent with the formation of either **14** or **17**. Nanavati and Silverman (37) used [7-^{3}H]PLP-reconstituted GABA-AT and

[6-^{14}C]vigabatrin and showed that denaturation of the inactivated enzyme releases PMP and the enamine adduct from **20** in a 75:25 ratio, thereby supporting the enamine mechanism as a minor pathway and either **14** (Scheme 3) or **17** (Scheme 4), both of which would release PMP upon denaturation, as the major pathway. Further studies on the reactivity and reactions of the major adduct (37) led to the conclusion that **14** was the actual inactivation adduct.

The crystal structure of vigabatrin bound to GABA-AT (Fig. 4, *B* and *C*) elucidates the structure of the covalent adduct as one in which Lys-329 is attached to the terminal carbon of the vinyl group as proposed in Scheme 3, effectively ruling out the mechanisms shown in Scheme 4. It is not possible to differentiate between the ternary adducts **13**-**15** based on the electron density (Fig. 4*B*) alone, and there may be even more than one tautomer present in the crystal. The geometry appears most relaxed for tautomer **15** with an (unconstrained) torsion angle around the N–CA aldimine linkage of −169° and a κ torsion angle of 1° resulting in coplanarity of the aldimine linkage with the pyridine ring and a favorable H-bond between the ionized NH^+ and $O3^-$. Structure **15** is not consistent with the biochemical result that after denaturation PMP is formed; instead the release of PLP would be predicted. Tautomerization from **15** to **14**, however, would lead to the observed release of PMP under the conditions of the denaturation, but it is not clear why that tautomerization should occur.

The crystal spectrum of GABA-AT after treatment with vigabatrin (Fig. 5*B*) is compatible with the presence of the less conjugated system of ketimine **14**, the aldimine **15** with a shifted ketoenamine/enolimine equilibrium, the aldimine species **12**, or species **11**. Because the cofactor is gradually released from the crystal (Fig. 5*B*, *inset*), one can conclude that there is no covalent linkage between the cofactor and the protein, which is in disagreement with the crystal structure. Apparently, the different ways the vigabatrin complex had to be produced for structure determination (complex formation in solution and subsequent crystallization) and for spectroscopic analysis (crystal soaking) are relevant for resolving this issue. We suggest that, in the soaked crystal, the reaction does not progress efficiently beyond the formation of the external aldimine (**12**), which would be the species that gets released with time. The next step (Scheme 3) would require rotation of the vinyl group toward the active site lysine, which may well be hindered by a reduced conformational flexibility of the active site due to crystal lattice constraints. For the reaction with GEG, such a conformational change is not required, and the reaction can proceed to form a stable ternary complex. Overall, these findings point out that crystalline proteins might not behave as in the soluble form, because small, but functionally essential conformational changes may be prevented or the equilibrium distribution of species may be perturbed, causing unanticipated reactivity (44, 68).

Why is only the Michael addition adduct (**14**) observed in the vigabatrin structure and not the enamine adduct (**20**)? Possibly, the Michael addition complex is thermodynamically more stable than the enamine adduct, which would thus have been lost over the time needed for crystallization. As a result, a partially occupied Michael complex would be left in the crystal. Indeed, test refinement of the model with a partially occupied adduct showed that the occupancy can be set as low as 75% without getting unreasonable *B*-values. This is consistent with the 75:25 ratio of Michael addition to enamine addition adducts previously observed (37). Alternatively, a small fraction of active sites containing the enamine adduct (**20**) would not contribute significantly to the observed density (which is the average over all active sites).

In summary, we have obtained high resolution crystal structures of GABA-AT inactivated by GEG and vigabatrin. Each of these structures has clarified the products of inactivation, which then allowed for the elucidation of the major mechanisms of inactivation. This approach does not require the tedious and time-consuming synthesis of radiolabeled compounds and structure elucidation by peptide mapping. Although peptide mapping and mass spectrometry are important tools to identify sites of modification, they do not provide precise adduct structure information of crystallography needed to aid in the elucidation of reasonable inactivation mechanisms. However, as a note of caution, had the inactivation mechanism for vigabatrin been based solely on the crystal structure, the minor enamine inactivation pathway would have been overlooked. The adduct structures described here will serve as a starting point for the development of mechanism-based inactivators and reversible inhibitors to target specifically GABA-AT. The native structure has already led to the design of a vigabatrin analog that is converted exclusively by the enamine mechanism (63).

Acknowledgments—Financial support of this research, given by the National Institutes of Health, the Italian Ministero dell'Istruzione, dell'Università e della Ricerca, and the Italian Consiglio Nazionale delle Ricerche, Progetto Finalizzato Biotecnologie, is gratefully acknowledged.

REFERENCES

1. McGeer, E. G., McGeer, P. L., and Thompson, S. (1983) in *Glutamine, Glutamate, and GABA in the Central Nervous System* (Hertz, L., Kvamme, E., McGeer, E. G., and Schousboe, A., eds) pp. 3–17, Liss, New York
2. Baxter, C. F., and Roberts, E. (1958) *J. Biol. Chem.* **233,** 1135–1139
3. Kwon, O. S., Park, J., and Churchich, J. E. (1992) *J. Biol. Chem.* **267,** 7215–7216
4. De Biase, D., Maras, B., Bossa, F., Barra, D., and John, R. A. (1992) *Eur. J. Biochem.* **208,** 351–357
5. Mehta, P. K., and Christen, P. (2000) *Adv. Enzymol. Relat. Areas Mol. Biol.* **74,** 129–184
6. Storici, P., Capitani, G., De Biase, D., Moser, M., John, R. A., Jansonius, J. N., and Schirmer, T. (1999) *Biochemistry* **38,** 8628–8634
7. Cooper, A. J. L. (1985) *Methods Enzymol.* **113,** 80–82
8. Karlsson, A., Fonnum, F., Malthe-Sorenssen, D., and Storm-Mathisen, J. (1974) *Biochem. Pharmacol.* **23,** 3053–3061
9. Gale, K. (1989) *Epilepsia* **30,** Suppl. 3, S1–S11
10. Rogawski, M. A., and Porter, R. J. (1990) *Pharmacol. Rev.* **42,** 223–286
11. McNamara, J. O. (1996) in *The Pharmacological Basis of Therapeutics* (Hardman, J. G., Limbird, L. E., Molinoff, P. B., Ruddon, R. W., and Gilman, A. G., eds) pp. 461–486, McGraw-Hill, New York
12. Bakay, R. A. E., and Harris, A. B. (1981) *Brain Res.* **206,** 387–404
13. Loyd, K. G., Munati, C., Bossi, L., Stoeffels, C., Talairach, J., and Morselli, P. L. (1981) in *Neurotransmission, Seizures, Epilepsy* (Morselli, P. L., Loescher, W., and Loyd, K. G., eds) pp. 325–338, Raven Press, New York
14. Butterworth, J., Yates, C. M., and Simpson, J. (1983) *J. Neurochem.* **41,** 440–447
15. Nishino, N., Fujiwara, H., Noguchi-Kuno, S.-A., and Tanaka, C. (1988) *Jpn. J. Pharmacol.* **48,** 331–339
16. Aoyagi, T., Wada, T., Nagai, M., Kojima, F., Harada, S., Takeuchi, T., Takahashi, H., Hirokawa, K., and Tsumita, T. (1990) *Chem. Pharm. Bull. (Tokyo)* **38,** 1748–1749
17. Gunne, L. M., Haeggstroem, J. E., and Sjoequist, B. (1984) *Nature (Lond.)* **309,** 347–349
18. Johnston, G. A. R., Curtis, D. R., Beart, P. M., Game, C. J. A., McColloch, R. M., and Twichin, B. (1975) *J. Neurochem.* **24,** 157–160
19. Schon, F., and Kelly, J. S. (1974) *Brain Res.* **66,** 289–300
20. Johnston, G. A. R., Stephanson, A. L., and Twichin, B. (1977) *J. Pharm. Pharmacol.* **29,** 240–241
21. Brehm, L., Hjeds, H., and Krogsgaard-Larsen, P. (1972) *Acta Chem. Scand.* **26,** 1298–1299
22. Krogsgaard-Larsen, P., Johnston, G. A. R., Lodge, D., and Curtis, D. R. (1977) *Nature* **268,** 53–55
23. Beart, P. M., Curtis, D. R., and Johnston, G. A. R. (1971) *Nat. New Biol.* **234,** 80–81
24. Silverman, R. B. (1995) *Methods Enzymol.* **249,** 240–283
25. Nanavati, S. M., and Silverman, R. B. (1989) *J. Med. Chem.* **32,** 2413–2421
26. Lippert, B., Metcalf, B. W., Jung, M. J., and Casara, P. (1977) *Eur. J. Biochem.* **74,** 441–445
27. Loscher, W. (1982) *Neuropharmacology* **21,** 803–810
28. Gidal, B. E., Privitera, M. D., Sheth, R. D., and Gilman, J. T. (1999) *Ann. Pharmacother.* **33,** 1277–1286
29. Kalviainen, R., and Nousiainen, I. (2001) *CNS Drugs* **15,** 217–230
30. John, R. A., Jones, E. D., and Fowler, L. J. (1979) *Biochem. J.* **177,** 721–728
31. Rando, R. R., and Bangerter, F. W. (1977) *Biochem. Biophys. Res. Commun.* **76,** 1276–1281
32. Fowler, L. J., and John, R. A. (1972) *Biochem. J.* **130,** 569–573

33. Dewey, S. L., Morgan, A. E., Ashby, C. R., Jr., Horan, B., Kushner, S. A., Logan, J., Volkow, N. D., Fowler, J. S., Gardner, E. L., and Brodie, J. D. (1998) *Synapse* **30,** 119–129
34. Burke, J. R., and Silverman, R. B. (1991) *J. Am. Chem. Soc.* **113,** 9329–9340
35. De Biase, D., Barra, D., Bossa, F., Pucci, P., and John, R. A. (1991) *J. Biol. Chem.* **266,** 20056–20061
36. Metcalf, B. W. (1979) *Biochem. Pharmacol.* **28,** 1705–1712
37. Nanavati, S. M., and Silverman, R. B. (1991) *J. Am. Chem. Soc.* **113,** 9341–9349
38. Collaborative computational project number 4 (1994) *Acta Crystallog. Sect. D.* **50,** 760–763
39. Winn, M. D., Isupov, M. N., and Murshudov, G. N. (2001) *Acta Crystallogr. D. Biol. Crystallogr.* **57,** 122–133
40. Cowtan, K. (1994) *Joint CCP4 and ESF-EACBM Newsletter on Protein Crystallography* **31,** 34–38
41. Stookey, L. L. (1970) *Anal. Chem.* **42,** 779–781
42. King, T. E., and Morris, R. O. (1967) *Methods Enzymol.* **10,** 631–641
43. Mozzarelli, A., Peracchi, A., Rossi, G. L., Ahmed, S. A., and Miles, E. W. (1989) *J. Biol. Chem.* **264,** 15774–15780
44. Mozzarelli, A., and Rossi, G. L. (1996) *Annu. Rev. Biophys. Biomol. Struct.* **25,** 343–365
45. Hofrichter, J., and Eaton, W. A. (1976) *Annu. Rev. Biophys. Bioeng.* **5,** 511–560
46. Phillips, R. S., Demidkina, T. V., Zakomirdina, L. N., Bruno, S., Ronda, L., and Mozzarelli, A. (2002) *J. Biol. Chem.* **277,** 21592–21597
47. Faeder, E. J., and Hammes, G. G. (1970) *Biochemistry* **9,** 4043–4049
48. Fu, W., Jack, R. F., Morgan, T. V., Dean, D. R., and Johnson, M. K. (1994) *Biochemistry* **33,** 13455–13463
49. John, R. A., Morgan, P. H., and Fowler, L. J. (1984) *Biochem. Soc. Trans.* **12,** 430–432
50. Churchich, J. E., and Moses, U. (1981) *J. Biol. Chem.* **256,** 1101–1104
51. Beinert, H., Holm, R. H., and Munck, E. (1997) *Science* **277,** 653–659
52. Shen, B. W., Hennig, M., Hohenester, E., Jansonius, J. N., and Schirmer, T. (1998) *J. Mol. Biol.* **277,** 81–102
53. Toney, M. D., Hohenester, E., Cowan, S. W., and Jansonius, J. N. (1993) *Science* **261,** 756–759
54. Beinert, H., and Kiley, P. J. (1999) *Curr. Opin. Chem. Biol.* **3,** 152–157
55. Paul, V., and Jayakumar, A. R. (2000) *Brain Res. Bull.* **51,** 43–46
56. Ollagnier-De-Choudens, S., Mulliez, E., Hewitson, K. S., and Fontecave, M. (2002) *Biochemistry* **41,** 9145–9152
57. Chen, D., and Frey, P. A. (2001) *Biochemistry* **40,** 596–602
58. Weyand, M., and Schlichting, I. (1999) *Biochemistry* **38,** 16469–16480
59. Silverman, R. B. (2002) *The Organic Chemistry of Enzyme-Catalyzed Reactions*, Academic Press, San Diego
60. John, R. A., and Fowler, L. J. (1976) *Biochem. J.* **155,** 645–651
61. McPhalen, C. A., Vincent, M. G., and Jansonius, J. N. (1992) *J. Mol. Biol.* **225,** 495–517
62. Clark, P. A., Jansonius, J. N., and Mehler, E. L. (1993) *J. Am. Chem. Soc.* **115,** 1894–1902
63. Choi, S., Storici, P., Schirmer, T., and Silverman, R. B. (2002) *J. Am. Chem. Soc.* **124,** 1620–1624
64. Jung, M. J., and Metcalf, B. W. (1975) *Biochem. Biophys. Res. Commun.* **67,** 301–306
65. Lippert, B., Jung, M. J., and Metcalf, B. W. (1980) *Brain Res. Bull.* **5,** Suppl. 2, 375–379
66. Jung, M. J., Lippert, B., Metcalf, B. W., Schechter, P. J., Bohlen, P., and Sjoerdsma, A. (1977) *J. Neurochem.* **28,** 717–723
67. Loscher, W. (1986) *Biochem. Pharmacol.* **35,** 3176
68. Mozzarelli, A., and Betatti, S. (2001) in *Advanced Functional Molecules and Polymers* (Nalwa, H. S., ed) Vol. 4, pp. 55–97, Gordon and Breach Science Publishers, Tokyo

Structures of γ-Aminobutyric Acid (GABA) Aminotransferase, a Pyridoxal 5′-Phosphate, and [2Fe-2S] Cluster-containing Enzyme, Complexed with γ-Ethynyl-GABA and with the Antiepilepsy Drug Vigabatrin

Paola Storici, Daniela De Biase, Francesco Bossa, Stefano Bruno, Andrea Mozzarelli, Caroline Peneff, Richard B. Silverman and Tilman Schirmer

J. Biol. Chem. 2004, 279:363-373.
doi: 10.1074/jbc.M305884200 originally published online October 8, 2003
